DIFFERENTIATION

Unbiased transcription factor CRISPR screen identifies ZNF800 as master repressor of enteroendocrine differentiation

Lin Lin[1,2,3]*, Jeff DeMartino[2,3], Daisong Wang[1,2], Gijs J. F. van Son[2,3], Reinier van der Linden[1,2], Harry Begthel[1,2], Jeroen Korving[1,2], Amanda Andersson-Rolf[1,2], Stieneke van den Brink[1,2], Carmen Lopez-Iglesias[4], Willine J. van de Wetering[4], Aleksandra Balwierz[3], Thanasis Margaritis[3], Marc van de Wetering[2,3], Peter J. Peters[4], Jarno Drost[2,3], Johan H. van Es[1,2], Hans Clevers[1,2,3]*†

Enteroendocrine cells (EECs) are hormone-producing cells residing in the epithelium of stomach, small intestine (SI), and colon. EECs regulate aspects of metabolic activity, including insulin levels, satiety, gastrointestinal secretion, and motility. The generation of different EEC lineages is not completely understood. In this work, we report a CRISPR knockout screen of the entire repertoire of transcription factors (TFs) in adult human SI organoids to identify dominant TFs controlling EEC differentiation. We discovered ZNF800 as a master repressor for endocrine lineage commitment, which particularly restricts enterochromaffin cell differentiation by directly controlling an endocrine TF network centered on PAX4. Thus, organoid models allow unbiased functional CRISPR screens for genes that program cell fate.

Enteroendocrine cells (EECs) are specialized epithelial cells of the intestinal tract that, like all other epithelial cell lineages, derive from regionally specified Lgr5$^+$ intestinal stem cells (ISCs) (*1*–*5*). Balanced differentiation of EEC lineages from ISCs is governed by a network of transcription factors (TFs) (*6*–*12*). RNA sequencing and organoid technology have illuminated the temporal hierarchy of gene expression profiles during EEC development (*13*, *14*). By using a time-resolved reporter allele of *Neurog3* (master regulator of endocrine development) (*15*, *16*), a real-time and lineage-specific map of mouse EEC differentiation in vivo was constructed at single cell–level resolution (*12*). Overexpression of *NEUROG3* can generate endocrine cells for functional characterization in human pancreatic duct cells (*17*). Leveraging human gut organoids, this strategy enabled profiling of EEC subtypes along the proximal-distal gastrointestinal axis (*18*). TFs known to specify EEC subtypes in mice were further examined in human organoids, revealing a predominantly conserved regulatory mechanism downstream of *NEUROG3* activation. However, discrepancies between mouse and human data were also observed. The regulatory mechanisms upstream of *NEUROG3* and the endogenous repressive factors that control *NEUROG3* expression at the adult stage remain largely unknown. In this work, we established an organoid-based platform in combination with high-throughput genetic screening for the unbiased discovery of TFs that govern human EEC lineage commitment.

Results

TFome-wide CRISPR knockout screen in human SI organoids

Optimized human SI organoids exhibit the spontaneous generation of all major cell lineages, including EEC subtypes, without TF overexpression (*19*). For the current study, we aimed to establish a CRISPR screening platform spanning the entire repertoire of transcription factors (TFome) in human intestinal organoids to allow for unbiased and systematic discovery of TFs that govern cell lineage commitment from adult LGR5$^+$ intestinal stem cells. We used a CRISPR knockout library comprising 7210 single-guide RNAs (sgRNAs) targeting 1800 human TFs, alongside 100 negative controls (*20*–*22*). In the human ileum organoid line used, EECs were marked by CHGA-IRES-iRFP670, goblet cells by MUC2-mNeonGreen, and Paneth cells by DEFA5-IRES-DsRed (fig. S1A). We performed lentiviral-mediated library integration in expanding SI organoids (Fig. 1A). Library coverage was assessed by sequencing the integrated sgRNAs, comparing the organoids after transduction with the plasmid pool.

Fate separation of CHGA$^+$ EECs and MUC2$^+$ cells occurs early in secretory progenitors, whereas DEFA5$^+$ Paneth cells emerge later from MUC2$^+$ progenitors (*19*), illustrating sequential fate decisions of ISCs (*23*, *24*). We aimed to track the early CHGA$^+$/MUC2$^+$ binary fate decision. After two-step organoid differentiation (*19*), we analyzed bulk populations as well as sorted EECs (CHGA$^+$), goblet cells (MU[illegible]) and the CHGA$^-$/MUC2$^-$/DEFA5$^-$ popula[illegible] (fig. S1B). 0 to ~0.7% sgRNAs yielded zero reads in bulk populations, indicating robust coverage (fig. S2A). Normalized read-count distribution and Pearson correlations demonstrated high concordance between biological replicates (fig. S2, B and C). sgRNAs that target essential ISC genes [*KLF5* (*25*) and *TCF7L2*/*TCF4* (*26*–*29*)] were depleted, along with "generic" cell fitness genes (*POLR2L*, *MYC*, and *RAD51*) at both expansion and differentiation culturing stages (β score < −1; FDR < 0.05 versus plasmid library) (fig. S2D and table S1). Furthermore, sgRNAs targeting *IRF2*, an interferon pathway TF, were highly enriched upon differentiation, consistent with existing literature (*30*, *31*).

sgRNAs were then assessed in CHGA$^+$ EECs and MUC2$^+$ goblet cells versus the triple reporter–negative cell population (Fig. 1B and table S2). As expected, *NEUROG3*, *SOX4*, and *INSM1* sgRNAs were depleted in EECs (*8*, *15*, *16*, *32*). Additionally, *NFIC*, *TEF*, and *ZHX2* appeared essential for EEC commitment. For each of these, clonal knockout organoids revealed a mild yet significant reduction of CHGA$^+$ EECs (Fig. 1, B and C, and fig. S3, A to C). Conversely, *GFI1* sgRNAs were enriched in EECs (Fig. 1, B and C). Mouse *Gfi1* is crucial for goblet cell differentiation by suppression of *Neurog3*-driven EEC cell fate (*23*, *33*). Indeed, *GFI1* knockout in human organoids abrogated goblet cell formation while increasing EEC numbers (fig. S3, A and C, and fig. S14, C and D).

ZNF800 represses EEC differentiation

The strongest repressor of EEC differentiation in the screen, *ZNF800*, is a C_2H_2 zinc-finger TF of unknown function (Fig. 1, B and C) (*34*). Human *ZNF800* is broadly expressed, including in the SI and colon epithelium (fig. S4, A and B). ZNF800$^{-/-}$ organoids contained increased EECs and strongly reduced goblet and Paneth cell numbers (Fig. 1, D and E, and fig. S4, C and G). Transmission electron microscopy confirmed the absence of goblet and Paneth cells with the characteristic apical secretory vesicles and the increase of EECs with the basolateral secretory granules (Fig. 1F). Similarly, ZNF800 knockout in colon organoid lines from two different donors also resulted in a significant increase in EECs (fig. S4, D to G).

We next performed single-cell RNA sequencing (scRNA-seq) to study the phenotype of ZNF800$^{-/-}$ organoids. For equal representation, CHGA$^+$ cells were sorted from wild type (WT) and ZNF800$^{-/-}$ organoids and pooled with CHGA$^-$ cells from the same lines in a 1:4 ratio (Fig. 2A and fig. S5A). Major intestinal cell types were identified by graph-based clustering analysis (Fig. 2B and fig. S5B). We observed the expected reduction of goblet cells

[1]Hubrecht Institute, Royal Netherlands Academy of Arts and Sciences (KNAW) and UMC Utrecht, Utrecht, Netherlands. [2]Oncode Institute, Utrecht, Netherlands. [3]Princess Maxima Center for Pediatric Oncology, Utrecht, Netherlands. [4]The Maastricht Multimodal Molecular Imaging Institute, Maastricht University, Maastricht, Netherlands.
*Corresponding author. Email: l.lin@hubrecht.eu (L.L.); h.clevers@hubrecht.eu (H.C.)
†Current address: Pharma Research and Early Development of F. Hoffmann–La Roche Ltd., Basel, Switzerland.

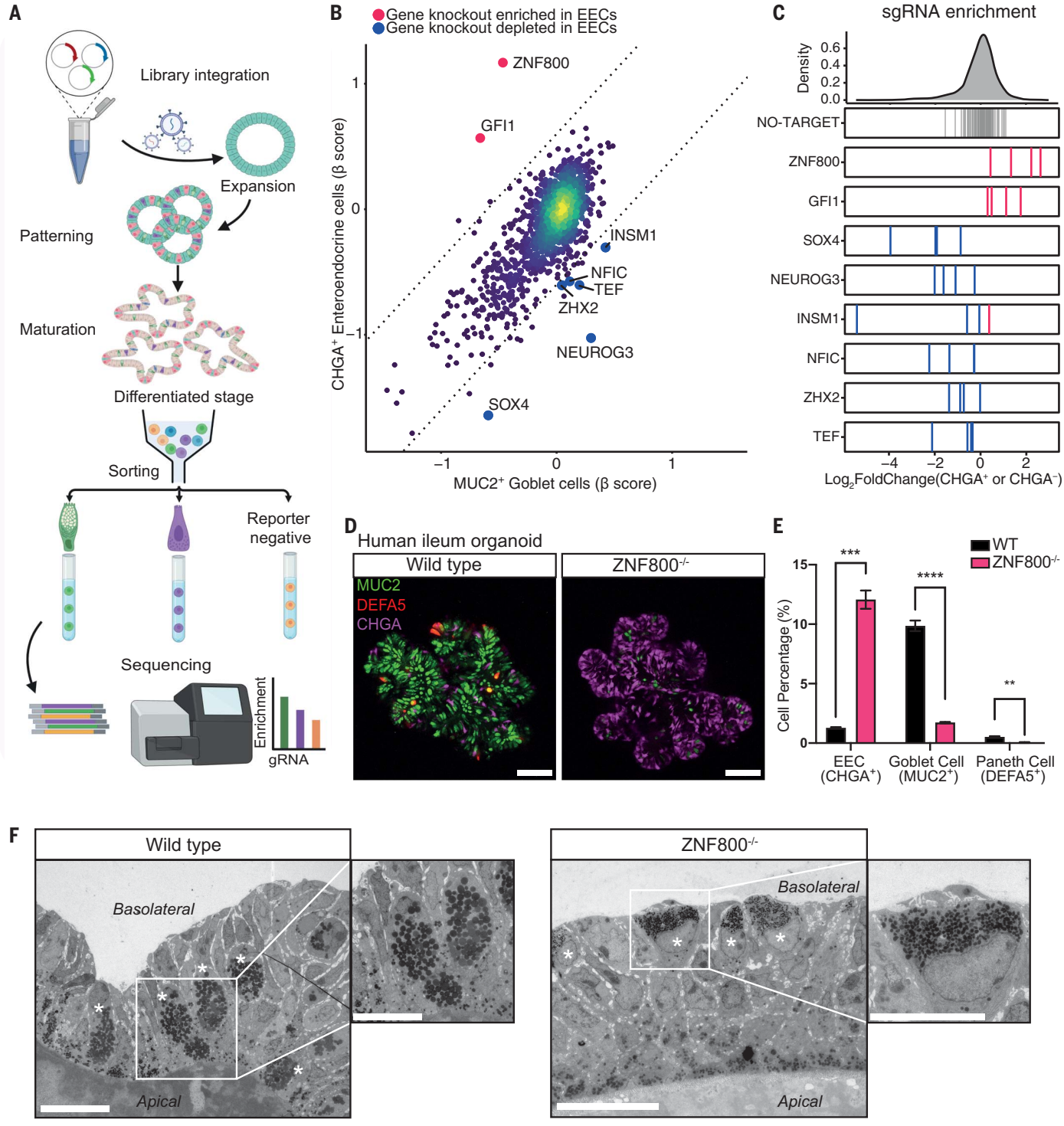

Fig. 1. TFome-wide CRISPR screen for endocrine differentiation in human SI organoids. (**A**) Schematic of TFome CRISPR screen. (**B**) Scatter plot of enrichment β score of each TF gene in CHGA$^+$ EECs and MUC2$^+$ goblet cells versus the triple reporter–negative cell population. (**C**) Individual sgRNA enrichment for genes of interest presented by $\log_2$-fold changes in CHGA$^+$ EECs versus triple reporter–negative cell population. Density plot (top) represents the distribution of nontargeting sgRNAs. (**D**) Representative confocal images of WT and ZNF800$^{-/-}$ human SI organoids. Representative marker genes for EECs (CHGA, magenta), goblet cells (MUC2, green), and Paneth cells (DEFA5, red) are highlighted by fluorescent reporters. Scale bars, 100 μm. (**E**) Proportion of different differentiated cell types as determined by FACS analysis of the respective reporters. Data are shown as mean ± SEM. $^{**}P < 0.01$; $^{***}P < 0.001$; $^{****}P < 0.0001$ by multiple *t* tests with two-stage linear step-up procedure of Benjamini, Krieger, and Yekutieli with $Q = 5\%$ and $n = 3$. (**F**) Transmission electron microscopy images of WT and ZNF800$^{-/-}$ human SI organoids. Goblet and Paneth cells are indicated with asterisks in WT organoids, and EECs are indicated with asterisks in ZNF800$^{-/-}$ organoids. Scale bars, 20 μm and 10 μm (zoom in).

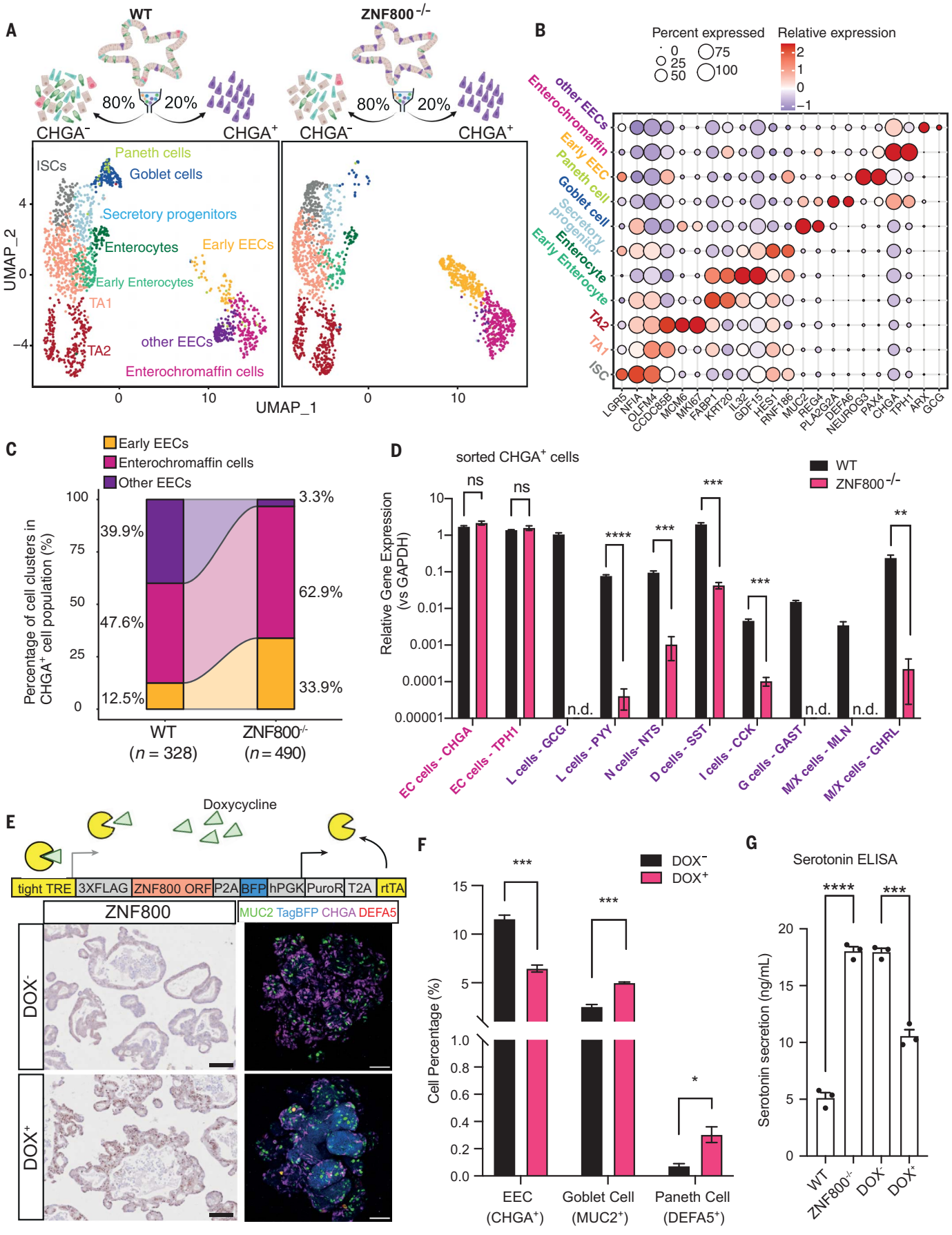

Fig. 2. Phenotypic characterization of ZNF800$^{-/-}$ organoids. (**A**) Uniform manifold approximation and projection (UMAP) of WT and ZNF800$^{-/-}$ organoids from scRNA-seq. Descriptive cluster labels are shown. TA1, transit-amplifying cell stage 1; TA2, transit-amplifying cell stage 2. (**B**) Dot plot showing the relative expression and the percentage of cells expressing selected markers across scRNA-seq clusters. Two representative markers for each cluster are plotted. (**C**) Stacked bar plot showing the EEC cell populations in WT and ZNF800$^{-/-}$ organoids. (**D**) Reverse transcription (RT)–qPCR quantification of various EEC markers in CHGA^{+} cell populations of WT and ZNF800$^{-/-}$ organoids. (**E**) (Top) Schematic of dox-inducible overexpression construct of ZNF800. (Bottom left) Representative immunohistochemical staining images of ZNF800 in ZNF800$^{-/-}$ organoids with or without dox-induced ZNF800 expression. (Bottom right) Representative confocal images of organoids with fluorescent reporters. Scale bars, 100 μm. (**F**) Proportion of EECs and goblet and Paneth cells as determined by fluorescence-activated cell sorting (FACS) analysis of the respective reporters in ZNF800$^{-/-}$ organoids with or without dox-induced ZNF800 expression. (**G**) Enzyme-linked immunosorbent assay (ELISA) quantification of serotonin secretion of organoids in different conditions. Data in this figure are shown as mean ± SEM. N.d. not detected; ns, not significant. *P < 0.05; **P < 0.01; ***P < 0.001; ****P < 0.0001 by multiple t tests with two-stage linear step-up procedure of Benjamini, Krieger, and Yekutieli with Q = 5% and n = 3.

in ZNF800$^{-/-}$ organoids (2.3%) compared with WT organoids (10.8%) (fig. S5C). Clonal formation efficiency of WT and ZNF800$^{-/-}$ SI and colon organoids revealed no significant differences (fig. S6, A and B). Cell-cycle progression in WT versus ZNF800$^{-/-}$ organoids using a Fucci cell-cycle reporter (*35*) showed no significant differences (fig. S6C). The combined results indicate that ZNF800 does not affect ISC homeostasis in organoids.

EECs were further subclustered based on markers of early EECs (*NEUROG3* and *PAX4*), enterochromaffin cells (ECs, *CHGA* and *TPH1*) and the other EEC subtypes (D cells, *SST*; L cells, *GCG* and *PYY*; M/X cells, *MLN* and *GHRL*; I cells, *CCK*; G cells, *GAST*; N cells, *NTS*) (Fig. 2B and fig. S7A). Notably, early EECs and ECs were increased in ZNF800$^{-/-}$ organoids, whereas other EEC subtypes were depleted (Fig. 2, C and D, and fig. S7A). The same phenotype was also observed in human colon organoids (fig. S8, A and B). Thus, *ZNF800* loss induces robust EEC differentiation at the expense of goblet cells while also driving an EC-biased trajectory.

We reexpressed WT ZNF800 protein in ZNF800$^{-/-}$ organoids by doxycycline (dox)–inducible overexpression (Fig. 2E and fig. S8C), which effectively rescued goblet and Paneth cell differentiation while repressing EEC lineage commitment (Fig. 2F). Notably, the EC-biased differentiation pattern was also reversed upon ZNF800 rescue, which resulted in decreased serotonin secretion, a hallmark hormone of ECs (Fig. 2G and fig. S8D).

ZNF800 represses the endocrine TF regulatory network

Differential gene expression (DGE) analysis in CHGA^{+} cell populations of WT and ZNF800$^{-/-}$ organoids highlighted distinct expression patterns of EEC-specific TFs (fig. S9, A and B). To unravel these gene regulatory mechanisms, we performed single-cell regulatory network inference and clustering (SCENIC) analysis on our scRNA-seq dataset (*36*), which identified 249 regulons activated across different cell clusters (table S4). Regulons controlling EEC commitment displayed higher activity in ZNF800$^{-/-}$ organoids, including *SOX4*, *NEUROD2*, and *PAX4* (Fig. 3A). Notably, *TEF* and *NFIC*, discovered in the TFome CRISPR screen as EEC regulators, also showed regulon activity in EEC lineages (fig. S9C), supporting the functional relevance of our hits.

Chromatin immunoprecipitation sequencing (ChIP-seq) with anti-ZNF800 and anti-FLAG antibodies revealed 11,565 consensus peaks in WT organoids and 7085 in rescued ZNF800$^{-/-}$ organoids (q value < 0.01) (fig. S10A). Most ZNF800-binding sites localized within ±5 kb of transcription start sites (TSS) (fig. S10B). Comparison between ZNF800 peak-proximal genes in WT organoids and in rescued ZNF800$^{-/-}$ organoids showed a clear overlap (Fig. 3B). Of the consensus 3625 ZNF800-binding genes, we captured 3085 (85%) in our scRNA-seq dataset (fig. S11A). DGE analysis (adjusted P value < 0.05) revealed that 461 (15%) of the ZNF800-bound genes were significantly upregulated upon ZNF800 knockout, whereas 59 (2%) were significantly down-regulated (fig. S11B and table S5), indicating that ZNF800 functions as a transcriptional repressor.

Gene ontology enrichment analysis of 870 genes (corresponding to the top 1000 anti-ZNF800 ChIP-seq peak loci) revealed enrichment of neural and endocrine-gland development pathways (fig. S11C and table S6). We then constructed an enrichment map for gene sets involved in gland development, endocrine system development, and pancreas development (Fig. 3C). In particular, *INSM1*, *NEUROG3*, and *PAX4* were found to be central TFs in each node with the highest ZNF800 binding activity. As predicted from SCENIC (Fig. 3A), ZNF800 bound *SOX4* and *NEUROD2* loci (Fig. 3D and fig. S12A). *EGR2* and *DLL3* were also prioritized as top hits by ZNF800 peak abundance; both are implicated in neurogenesis (*37*–*41*) and specifically expressed in endocrine cell lineages (fig. S12B). These findings were highly correlated with their respective gene expression profiles (fig. S10C and S12B). Notably, we also identified mild enrichment of ZNF800 binding activity on the *NEUROD1* locus (fig. S12A). Knockout of *ZNF800* resulted in increased gene expression of *NEUROD1* (fig. S11B). However, *NEUROD1* did not appear as a hit in our CRISPR screen (fig. S12C). *Neurod1* acts as a late-stage EEC TF in mice (*12*). In human EECs, *NEUROD1* was also found to mark late progenitors and mature EECs (*18*). We therefore generated NEUROD1$^{-/-}$ organoids, which exhibited no effect on EEC or goblet cell differentiation (fig. S12, D to F), whereas profiling of EEC subtypes demonstrated a mild decrease in ECs, G cells, and M/X cells and a mild increase in N cells (fig. S12G). These results confirmed that *NEUROD1* is a late-stage TF regulator, which does not affect the EEC or goblet binary cell–fate decision.

Most ZNF800-binding loci presented a bivalent (H3K4me3- and H3K27me3-containing) chromatin signature in the SI and colon (Fig. 3D and fig. S13A). Such marks are associated with stem-cell differentiation, allowing timely responsiveness to TF regulation (*42*, *43*). The reversibility of gene activation or suppression by poised ZNF800-binding loci was tested in organoids with inducible ZNF800 expression (fig. S13B). Sequential cycles of dox induction demonstrated that ZNF800 alone can trigger a dynamic yet reversible equilibrium between EECs and goblet cells.

GFI1 and ZNF800 function independently in repressing EEC differentiation

Given that both ZNF800 and GFI1 were discovered in our screen as repressors of EEC differentiation, we sought to understand their regulatory interactions by generating a double knockout of *GFI1* and *ZNF800* (GFI1$^{-/-}$;ZNF800$^{-/-}$) in human SI organoids (fig. S14A). Further abrogation of goblet and Paneth cells was observed in GFI1$^{-/-}$;ZNF800$^{-/-}$ organoids (fig. S14, C and D), mirrored by further induction of EECs. The GFI1$^{-/-}$ single knockout did not lead to EC bias (fig. S14E). Instead, we observed a mild decrease of EC cells (*TPH1*) and a subtle increase in L cells (*PYY*). Notably, ZNF800 expression was not affected by *GFI1* loss (fig. S14, B and E). Because GFI1 is expressed in goblet and Paneth cells (*33*) and the knockout of *ZNF800* significantly depleted both cell types, we assayed GFI1 expression in goblet cells sorted from WT (12 ± 1.0%) and ZNF800$^{-/-}$ (3.4 ± 0.14%) organoids to avoid biased cell heterogeneity of the organoids, which revealed no differences in GFI1 expression (fig. S14F). Overall, our results indicated that ZNF800 and GFI1 function independently as repressors of EEC differentiation.

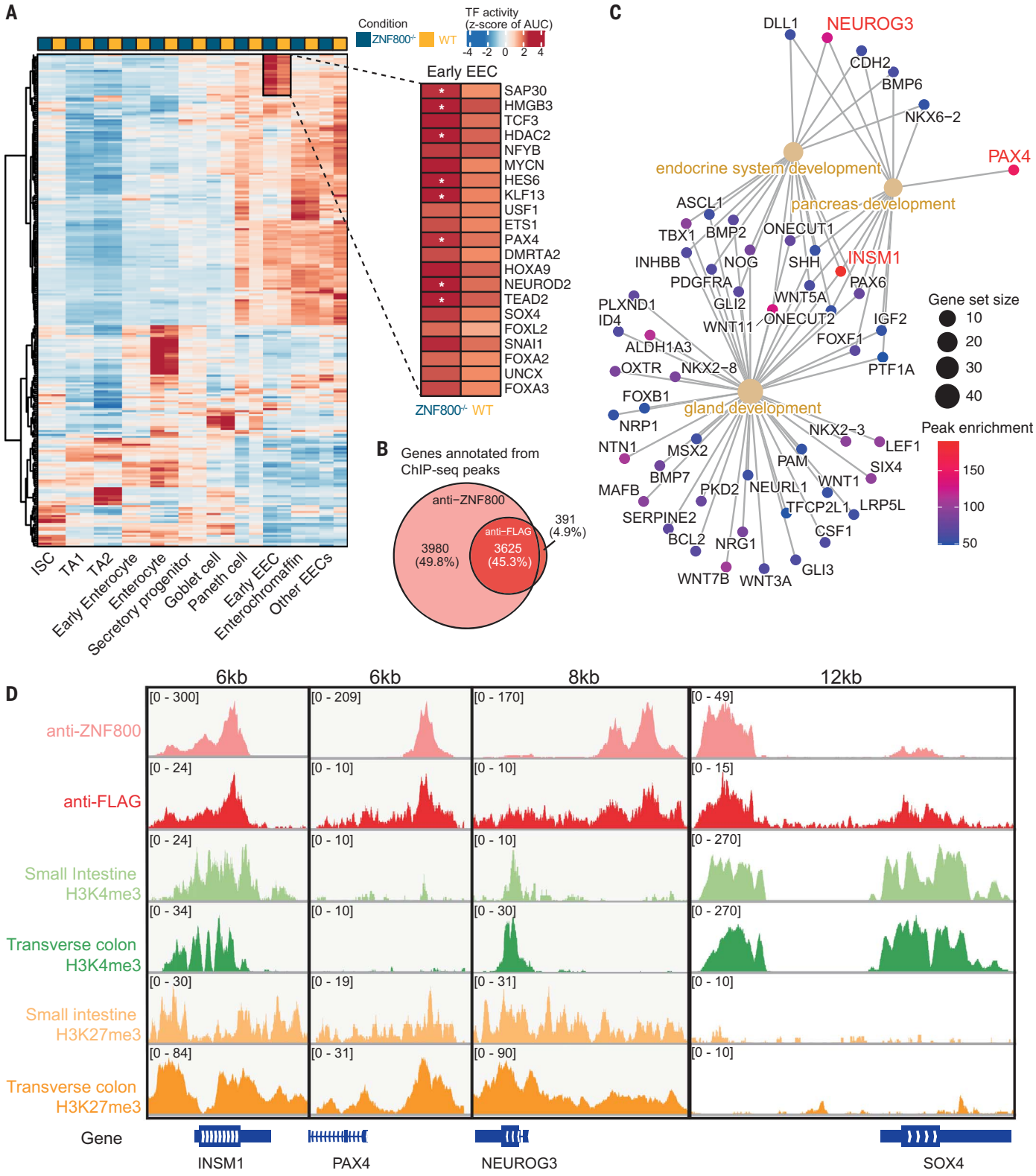

Fig. 3. ZNF800 binds to chromatin regions of TFs involved in endocrine differentiation. (**A**) Heatmap with unsupervised clustering of gene regulatory network activity in different cell clusters within WT and ZNF800$^{-/-}$ organoids and visualized as row *z*-scores of mean area-under-the-curve (AUC) values. Zoom-in plot highlighting the top TF regulons specifically activated in early EECs. Regulons with significant differences between WT and ZNF800$^{-/-}$ are indicated with asterisks, assessed by Wilcoxon rank sum test. (**B**) Venn diagram of overlapping genes annotated from ChIP-seq datasets generated by anti-ZNF800 antibody in WT organoids and anti-FLAG antibody in ZNF800$^{-/-}$ organoids with dox-induced ZNF800 expression. (**C**) An enrichment-network plot depicting the linkages of gene sets and three selected pathways by gene ontology analysis. (**D**) ChIP-seq tracks at the *INSM1*, *PAX4*, *NEUROG3*, and *SOX4* loci.

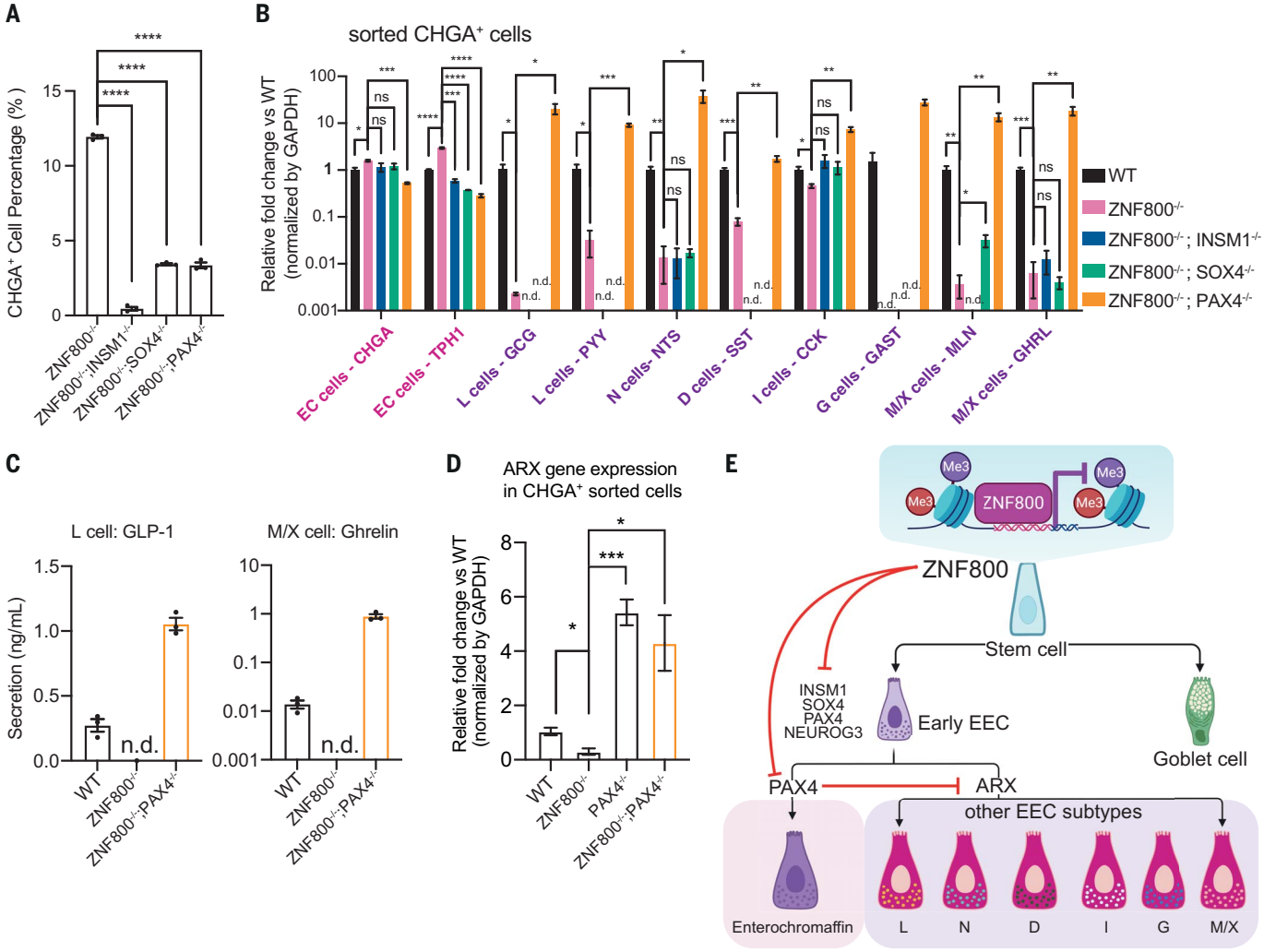

Fig. 4. PAX4 is responsible for EC-biased differentiation trajectory as a direct downstream target of ZNF800. (**A**) Proportions of EECs as determined by FACS analysis of organoids from different genotypes by CHGA reporter. (**B**) RT-qPCR quantification of various EEC markers in CHGA$^+$ cell populations of organoids from different genotypes. (**C**) ELISA quantification of GLP-1 and Ghrelin secretion of organoids from different genotypes. (**D**) RT-qPCR quantification of ARX expression in CHGA$^+$ cell populations of organoids from different conditions. (**E**) Schematic of ZNF800-driven repression model during endocrine cell differentiation. Data in this figure are shown as mean ± SEM. N.d. not detected; ns, not significant. *P < 0.05; **P < 0.01; ***P < 0.001; ****P < 0.0001 by multiple t tests with two-stage linear step-up procedure of Benjamini, Krieger, and Yekutieli with Q = 5%, n = 3.

PAX4 drives EC differentiation directly downstream of ZNF800

A panel of genes was found to be up-regulated across multiple cell types upon ZNF800 knockout (table S7), including *COL4A2*, *TMEM178B*, and *BTBD11* (fig. S15A). ZNF800 binds to these genes, but not to the down-regulated genes such as *SULT1C2*, *HMGCS1*, and *MS4A8* (fig. S15B). Despite their modest up-regulation, the expression pattern and the annotated function of these genes did not directly relate to the EEC phenotype. Therefore, we focused on EEC TFs with stronger functional implications (fig. S9, A and B).

We focused on three direct ZNF800 target genes, *INSM1*, *SOX4*, and *PAX4* (Fig. 3D), by performing double knockouts (fig. S16A). EEC induction was effectively suppressed, but to different extents (Fig. 4A). Similar to the single depletion of *INSM1* (fig. S3C), *INSM1* knockout in ZNF800$^{-/-}$ organoids caused an essentially complete reversal of EEC induction, confirming its pivotal role in the TF cascade (*8*, *44*). Additional knockout of *SOX4* or *PAX4* in ZNF800$^{-/-}$ organoids both reduced EEC numbers.

Next, we analyzed EEC subtypes in the CHGA$^+$ cell population from different mutant backgrounds (Fig. 4B and fig. S17, A and B). Additional knockout of *INSM1* or *SOX4* caused a mild reduction of EC cells (*TPH1*) in CHGA$^+$ cells while further suppressing L cells (*GCG* and *PYY*) and D cells (*SST*). Loss of *PAX4* directed a robust conversion of EC-biased EECs into all other EEC subtypes. Basal secretion of subtype hormones (L cell, GLP-1; M/X cell, Ghrelin), confirmed their functionality (Fig. 4C). We also performed a single knockout of *SOX4* and *PAX4* (fig. S3A, S16B and S18A). The SOX4$^{-/-}$ single knockout significantly repressed L cells (*GCG*), N cells (*NTS*), D cells (*SST*), and G cells (*GAST*), whereas MLN-expressing M/X cells were not affected, agreeing with findings in *Sox4*$^{-/-}$ mice (*12*) (fig. S18, B to D). The PAX4$^{-/-}$ single knockout repressed ECs while mildly up-regulating other EEC subtypes. Overall, *PAX4*, as a direct target of *ZNF800*, appeared responsible for the EC-biased EEC differentiation trajectory seen upon loss of *ZNF800*.

Mouse ECs are exclusively *Pax4*-dependent (*45*), whereas *Arx* is essential for L, G, I, and N cells (*10*, *45*). We therefore probed a possible interaction between PAX4 and ARX in our organoids. ARX expression was down-regulated in ZNF800$^{-/-}$ organoids and up-regulated in

PAX4$^{-/-}$ single-knockout and ZNF800$^{-/-}$;PAX4$^{-/-}$ double-knockout organoids (Fig. 4D and fig. S19, A and B). Reintroduction of PAX4 in ZNF800$^{-/-}$;PAX4$^{-/-}$ organoids significantly repressed ARX expression (fig. S20, A and B). Furthermore, as expected, the EEC differentiation trajectory in ZNF800$^{-/-}$;PAX4$^{-/-}$ organoids was redirected to an EC-biased phenotype upon PAX4 reexpression.

Reciprocal transcriptional repression exists between *Pax4* and *Arx* during mouse pancreatic development (*46*, *47*). We assessed whether ARX also inhibits intestinal PAX4 expression by overexpressing ARX in ZNF800$^{-/-}$ organoids (fig. S21A). ARX overexpression was insufficient to reverse the EC-biased EEC cell type specification induced by the ZNF800-PAX4 axis (fig. S21, B and C). Furthermore, PAX4 expression was not affected upon ARX overexpression in the ZNF800$^{-/-}$ condition (fig. S21D). We next performed ChIP-qPCR of ARX on the PAX4 locus using FLAG-tagged ARX in human SI organoids (fig. S21E). Unlike ZNF800, ARX did not bind to the PAX4 upstream enhancer region (fig. S21F). We also performed ChIP-qPCR of PAX4 on the ARX locus using FLAG-tagged PAX4 (fig. S22A), focusing on six ultraconserved enhancers (*48*–*50*) (fig. S22B). PAX4 did not bind across these enhancers, including hs121, which exhibits PAX4 binding activity in the mouse pancreas (fig. S22C) (*49*). Overall, our results strongly supported that PAX4 unilaterally inhibits ARX, whereas the inhibitory effect does not involve direct chromatin interaction through the previously described regulatory elements.

Discussion

The human SI epithelium consists of at least 14 main cell types, including six EEC lineages (*51*, *52*). Leveraging the near-physiological cell heterogeneity of human SI organoids, we performed a CRISPR screen for positive and negative TF regulators of EEC lineage commitment. Our findings define a ZNF800-repressive mechanism upstream of the classic endocrine gene regulatory network (Fig. 4E). Among its direct downstream targets, *INSM1*, *SOX4*, and *NEUROG3* are well described central players that drive early EEC commitment. We also found that PAX4, in the absence of ZNF800, drives an EC-specific cell fate by suppressing differentiation of all other EEC subtypes.

The *PAX4* knockout rescued somatostatin-producing D cells in ZNF800$^{-/-}$ organoids (Fig. 2D and fig. S7A). Although *Pax4* controls both β- and somatostatin-producing δ-cell specification in the mouse pancreas (*46*), our single *PAX4* knockout had no effect on SST-expressing D cells (fig. S18C). This prompts questions into the generalizability of endocrine fate regulation between different digestive organs. Double depletion of *Pax4* and *Arx* promoted δ-cell specification in mice (*49*), suggesting that a third TF is involved in δ-cell cell differentiation, and that *Pax4* is likely to induce a β-cell fate at the expense of δ cells. Therefore, the up-regulation of *PAX4* by ZNF800$^{-/-}$ in human SI organoids might drive a further binary cell–fate decision between ECs and D cells.

ZNF800 is ubiquitously expressed along the crypt-villus axis in the adult human gut epithelium (fig. S4A), marked by H3K4me3 enrichment and low H3K27me3 levels (fig. S4B), indicating an open chromatin state and active expression. The scRNA-seq dataset of the developing human gut revealed that ZNF800 is already expressed at the earliest assayed time point of 6.1 postconception weeks (*53*). Given the downstream TF network described in our study, it appears likely that ZNF800 also plays an important function in embryonic development. A recent coexpression network study in mouse pancreatic development (*54*) revealed that expression of the mouse ortholog *zfp800* correlates with endocrine specification from embryonic day 8 (E8) until E15.5. Global knockout of *zfp800* caused postnatal lethality and disrupted early pancreatic development (including both endocrine and acinar cells at E18.5). Thus, the constitutive null phenotype hindered a mechanistic study of mouse *zfp800* function in the endocrine lineages. It is conceivable that ZNF800 might regulate β-cell differentiation in the human pancreas through the TF network described in this study.

REFERENCES AND NOTES

1. N. Barker *et al*., *Nature* **449**, 1003–1007 (2007).
2. Y. Sei, X. Lu, A. Liou, X. Zhao, S. A. Wank, *Am. J. Physiol. Gastrointest. Liver Physiol.* **300**, G345–G356 (2011).
3. S. J. A. Buczacki *et al*., *Nature* **495**, 65–69 (2013).
4. O. Basak *et al*., *EMBO J.* **33**, 2057–2068 (2014).
5. O. Basak *et al*., *Cell Stem Cell* **20**, 177–190.e4 (2017).
6. H. Mutoh *et al*., *Proc. Natl. Acad. Sci. U.S.A.* **94**, 3560–3564 (1997).
7. F. J. Naya *et al*., *Genes Dev.* **11**, 2323–2334 (1997).
8. M. S. Gierl, N. Karoulias, H. Wende, M. Strehle, C. Birchmeier, *Genes Dev.* **20**, 2465–2478 (2006).
9. S. Desai *et al*., *Dev. Biol.* **313**, 58–66 (2008).
10. A. Du *et al*., *Dev. Biol.* **365**, 175–188 (2012).
11. S. Gross *et al*., *Development* dev.130682 (2016).
12. H. Gehart *et al*., *Cell* **176**, 1158–1173.e16 (2019).
13. T. Sato *et al*., *Nature* **459**, 262–265 (2009).
14. T. Sato *et al*., *Gastroenterology* **141**, 1762–1772 (2011).
15. G. Gradwohl, A. Dierich, M. LeMeur, F. Guillemot, *Proc. Natl. Acad. Sci. U.S.A.* **97**, 1607–1611 (2000).
16. M. Jenny *et al*., *EMBO J.* **21**, 6338–6347 (2002).
17. J. Lee *et al*., *eLife* **2**, e00940 (2013).
18. J. Beumer *et al*., *Cell* **181**, 1291–1306.e19 (2020).
19. G.-W. He *et al*., *Cell Stem Cell* **29**, 1333–1345.e6 (2022).
20. J. G. Doench *et al*., *Nat. Biotechnol.* **34**, 184–191 (2016).
21. S. A. Lambert *et al*., *Cell* **172**, 650–665 (2018).
22. L. Lin *et al*., *Cell Rep.* **33**, 108426 (2020).
23. N. F. Shroyer, D. Wallis, K. J. T. Venken, H. J. Bellen, H. Y. Zoghbi, *Genes Dev.* **19**, 2412–2417 (2005).
24. T. K. Noah, B. Donahue, N. F. Shroyer, *Exp. Cell Res.* **317**, 2702–2710 (2011).
25. T. Nakaya *et al*., *Cancer Res.* **74**, 2882–2891 (2014).
26. V. Korinek *et al*., *Nat. Genet.* **19**, 379–383 (1998).
27. E. Batlle *et al*., *Cell* **111**, 251–263 (2002).
28. M. van de Wetering *et al*., *Cell* **111**, 241–250 (2002).
29. J. H. van Es *et al*., *Mol. Cell. Biol.* **32**, 1918–1927 (2012).
30. K. Minamide *et al*., *Sci. Rep.* **10**, 14639 (2020).
31. T. Sato *et al*., *Nat. Cell Biol.* **22**, 919–926 (2020).
32. A. D. Gracz *et al*., *Gastroenterology* **155**, 1508–1523.e10 (2018).
33. M. Bjerknes, H. Cheng, *Dev. Biol.* **345**, 49–63 (2010).
34. H. S. Najafabadi *et al*., *Nat. Biotechnol.* **33**, 555–562 (2015).
35. A. Sakaue-Sawano *et al*., *Cell* **132**, 487–498 (2008).
36. S. Aibar *et al*., *Nat. Methods* **14**, 1083–1086 (2017).
37. M. H. Sham *et al*., *Cell* **72**, 183–196 (1993).
38. J. Ghislain, C. Desmarquet-Trin-Dinh, P. Gilardi-Hebenstreit, P. Charnay, M. Frain, *Development* **130**, 941–953 (2003).
39. A. Desmazières, P. Charnay, P. Gilardi-Hebenstreit, *J. Biol. Chem.* **284**, 10831–10840 (2009).
40. S. L. Dunwoodie, D. Henrique, S. M. Harrison, R. S. P. Beddington, *Development* **124**, 3065–3076 (1997).
41. R. M. Henke, D. M. Meredith, M. D. Borromeo, T. K. Savage, J. E. Johnson, *Dev. Biol.* **328**, 529–540 (2009).
42. B. E. Bernstein *et al*., *Cell* **125**, 315–326 (2006).
43. P. Voigt, W.-W. Tee, D. Reinberg, *Genes Dev.* **27**, 1318–1338 (2013).
44. A. B. Osipovich *et al*., *Development* **141**, 2939–2949 (2014).
45. A. Beucher *et al*., *PLOS ONE* **7**, e36449 (2012).
46. P. Collombat *et al*., *Genes Dev.* **17**, 2591–2603 (2003).
47. P. Collombat *et al*., *Cell* **138**, 449–462 (2009).
48. G. Bejerano *et al*., *Science* **304**, 1321–1325 (2004).
49. P. Collombat *et al*., *Development* **132**, 2969–2980 (2005).
50. D. E. Dickel *et al*., *Cell* **172**, 491–499.e15 (2018).
51. R. Elmentaite *et al*., *Nature* **597**, 250–255 (2021).
52. J. Burclaff *et al*., *Cell. Mol. Gastroenterol. Hepatol.* **13**, 1554–1589 (2022).
53. R. Elmentaite *et al*., *Dev. Cell* **55**, 771–783.e5 (2020).
54. A. B. Osipovich *et al*., *Development* **148**, dev196964 (2021).
55. ENCODE Project Consortium, *Nature* **489**, 57–74 (2012).
56. Y. Luo *et al*., *Nucleic Acids Res.* **48** (D1), D882–D889 (2020).

ACKNOWLEDGMENTS

We thank R. Sherwood (Harvard Medical School, Brigham and Women's Hospital, Division of Genetics) for providing the TFome sgRNA library in the CRISPR-v2-FE backbone. We thank D. Krueger, A. de Graaff, and the Hubrecht Imaging Centre for microscopy assistance and the Hubrecht Flow Cytometry Core Facility for flow cytometry analysis and cell sorting. We thank the Máxima Single Cell Genomics Facility and Utrecht Sequencing Facility for sequencing support. We thank the Microscopy CORE Lab of the Faculty of Health, Medicine, and Life Sciences of Maastricht University for its help in transmission electron microscopy imaging. We thank the ENCODE Consortium and the ENCODE production laboratories (B. Bernstein, Broad; J. Stamatoyannopoulos, UW; B. Ren, UCSD) for generating the related ChIP-seq public datasets. **Funding:** This work was supported by the Netherlands Organ-on-Chip Initiative, a Dutch Research Council (NWO) Gravitation project (024.003.001) funded by the Ministry of Education, Culture, and Science of the government of the Netherlands (H.C.); the Oncode Institute (partly financed by the Dutch Cancer Society) (H.C. and J.H.v.E.); and the European Research Council under ERC advanced grant no. 101020405 (GutHormones) (H.C.). The project Organoids in time with project no. 2019.085 of the research program NWO Investment Large is financed by the NWO (H.C. S.v.d.B.). **Author contributions:** Conceptualization: L.L. and H.C.; Methodology: L.L., J.De., D.W., G.J.F.v.S., R.v.d.L., H.B., J.K., S.v.d.B., A.A.-R., C.L.-I., W.J.v.d.W., A.B., T.M., M.v.d.W., P.J.P., J.Dr., J.H.v.E., and H.C.; Investigation: L.L., J.De., G.J.F.v.S., H.B., J.K., A.A.-R., C.L.-I., and W.J.v.d.W.; Visualization: L.L., J.De., G.J.F.v.S., and C.L.-I.; Funding acquisition: J.H.v.E. and H.C.; Project administration: J.H.v.E. and H.C.; Supervision: J.H.v.E. and H.C.; Writing – original draft: L.L. and H.C.; Writing – review and editing: all authors. **Competing interests:** H.C. is an inventor on patents held by the Royal Netherlands Academy of Arts and Sciences that cover organoid technology. He is currently head of pharma Research and Early Development (pRED) at

Roche, Basel, Switzerland. H.C.'s full disclosure is given at https://www.uu.nl/staff/JCClevers/. **Data and materials availability:** Further information and requests for resources and reagents should be directed to the corresponding author. Specific and stable reagents generated in this study are available and can be requested from the corresponding author; a completed Materials Transfer Agreement may be required. Sharing organoid lines used in this study requires approval by our local institutional review board. CRISPR screen sequencing data, scRNA-seq data, and ChIP-seq data from this study have been deposited to the Gene Expression Omnibus (GEO) under accession no. GSE229586. ChIP-seq data for histone marks H3K4me3 and H3K27me3 from human small intestine and colon were obtained from the ENCODE portal. We downloaded the ChIP-seq datasets from the ENCODE portal (*55*, *56*) (https://www.encodeproject.org/) with the following identifiers: ENCFF661MCT, ENCFF988AAQ, ENCFF219ZIO, ENCFF284XHG, ENCFF603QDZ, ENCFF825TAZ, ENCFF745IGA, and EENCFF830NSP.

SUPPLEMENTARY MATERIALS

science.org/doi/10.1126/science.adi2246
Materials and Methods
Figs. S1 to S22
References (*57*–*76*)
Tables S1 to S8
MDAR Reproducibility Checklist

Submitted 17 April 2023; resubmitted 9 August 2023
Accepted 8 September 2023
10.1126/science.adi2246

Unbiased transcription factor CRISPR screen identifies ZNF800 as master repressor of enteroendocrine differentiation

Lin Lin, Jeff DeMartino, Daisong Wang, Gijs J. F. van Son, Reinier van der Linden, Harry Begthel, Jeroen Korving, Amanda Andersson-Rolf, Stieneke van den Brink, Carmen Lopez-Iglesias, Willine J. van de Wetering, Aleksandra Balwierz, Thanasis Margaritis, Marc van de Wetering, Peter J. Peters, Jarno Drost, Johan H. van Es, and Hans Clevers

Science **382** (6669), . DOI: 10.1126/science.adi2246

Editor's summary

Enteroendocrine cells (EECs) reside in the epithelium of the digestive tract and produce various hormones involved in metabolism. The generation of different EEC lineages is governed by a dedicated network of transcription factors. However, given the low efficiency of EEC specification from adult stem cells, it has been difficult to elucidate the components of this regulatory network. Lin *et al*. used an optimized human small intestinal organoid culture system to perform an unbiased, systematic screen for transcription factors that regulate EEC differentiation. The screen implicated ZNF800 as a key factor exerting a dominant repressive role in controlling the endocrine transcription factor network. This work showcases the use of optimized human organoids for CRISPR-based functional screens, paving the way for the identification of additional regulators in human gut physiology and pathophysiology. —Stella M. Hurtley